Computer Assisted Mechanics and Engineering Sciences, 8: 271–288, 2001.


# An indirect Trefftz method for the steady-state dynamic analysis of coupled vibro-acoustic systems

Wim Desmet, Paul Sas and Dirk Vandepitte
*Katholieke Universiteit Leuven, Department of Mechanical Engineering, Division PMA*
*Celestijnenlaan 300 B, B-3001 Leuven, Belgium*

(Received June 30, 2000)

A new prediction technique, based on the indirect Trefftz method, has been developed for the steady-state dynamic analysis of coupled vibro-acoustic systems. In contrast with the finite element method, in which the dynamic field variables within each element are expanded in terms of local, non-exact shape functions, the dynamic field variables are expressed as global wave function expansions, which exactly satisfy the governing dynamic equations. The contributions of the wave functions to the coupled vibro-acoustic response result from a weighted residual formulation of the boundary conditions.

This paper discusses the basic principles and convergence properties of the new prediction technique and illustrates its performance for some two-dimensional validation examples. A comparison with the finite element method indicates that the new prediction method has a substantially higher convergence rate. This makes the method suitable for accurate coupled vibro-acoustic predictions up to much higher frequencies than the finite element method.

## 1. Introduction

At present, the finite element and boundary element method are the most commonly used numerical prediction techniques for solving steady-state dynamic problems, defined in structural and acoustic continuum domains. An important implication of the conventional element concept, using non-exact shape functions, is that the involved large model sizes practically restrict the applicability of these deterministic prediction techniques to the low-frequency range. Above a certain frequency limit, these methods would require, even with the nowadays-available high-performance computer resources, a prohibitively large amount of computational effort and memory resources to get an acceptable level of prediction accuracy.

For coupled vibro-acoustic problems, the conflict between computational effort and accuracy is even more pronounced than for uncoupled structural or uncoupled acoustic problems. First of all, the size of coupled prediction models is substantially larger, since a structural and an acoustic problem must be solved simultaneously to incorporate the acoustic pressure loading on the elastic structure and the continuity of the normal fluid and structural displacements along the fluid–structure coupling interface. Secondly, the numerical solution procedure for coupled vibro-acoustic models is less efficient than for uncoupled structural or uncoupled acoustic models, since coupled models, at least in their most commonly used acoustic pressure/structural displacement formulation [1], are no longer symmetric. Finally, the efficiency of the modal expansion method in reducing the model size is significantly reduced for coupled vibro-acoustic problems. The most appropriate mode selection for a modal expansion is the use of the modes of the coupled system. However, since coupled models are no longer symmetric, the calculation of coupled modes requires a non-symmetric eigenvalue calculation, which is very time consuming and which makes it a practically impossible procedure for many real-life vibro-acoustic problems. The most commonly used alternative is a modal expansion in terms of uncoupled structural and uncoupled acoustic modes, which result from computationally efficient symmetric eigenvalue problems. However, the fact that uncoupled acoustic modes have

a zero displacement component, normal to the fluid–structure coupling interface, implies that a large number of high-order uncoupled acoustic modes is required to accurately represent the normal displacement continuity along the fluid–structure interface. Hence, the benefit of a computationally efficient construction of the modal base is significantly reduced by the smaller model size reduction, obtained with an uncoupled modal base.

As a result, there exists still a substantial discrepancy between the limited frequency range, in which conventional element based models can provide accurate coupled vibro-acoustic predictions, and the significantly larger frequency range, in which accurate, deterministic predictions are needed for many industrial engineering problems.

In view of narrowing this currently existing frequency discrepancy, a new deterministic prediction technique has been developed [2], which is based on the indirect Trefftz method [5, 8].

The steady-state dynamic field variables in the entire — or at least in large subdomains of the — acoustic and structural domains of a coupled vibro-acoustic system are approximated in terms of a set of acoustic and structural wave functions, which are exact solutions of the homogeneous parts of the governing dynamic equations, and some particular solution functions of the inhomogeneous equations. In this way, the governing dynamic equations are exactly satisfied, irrespective of the contributions of the wave functions to the field variable expansions.

Since the proposed field variable expansions are exact solutions of the governing dynamic equations, the contributions of the wave functions to the field variable expansions are merely determined by the acoustic and structural boundary conditions. Since only finite sized prediction models are amenable to numerical implementation, the boundary conditions can only be satisfied in an approximate way. Therefore, the wave function contributions result from a weighted residual formulation of the boundary conditions.

A key issue in the use of the indirect Trefftz method is the definition of a T-complete function set, which ensures the convergence of the subsequent field variable expansions towards the exact solutions. Several T-complete function sets have already been defined for solving steady-state acoustic problems [3, 7] and steady-state dynamic plate bending problems [6]. Although the theoretical convergence for these function sets has been proven, their practical convergence is, however, seriously disturbed or even prevented, due to the ill-conditioning of the involved model matrices. The innovative character of the new prediction technique consists mainly of using a new class of T-complete wave functions, which allow the use of the indirect Trefftz method for coupled vibro-acoustic prediction models, whose poor condition is no longer preventing the numerical results from converging towards the exact solution.

This paper presents the basic principles of the new prediction technique and applies it for the vibro-acoustic modelling of some two-dimensional validation examples. It follows from these applications that a high accuracy is obtained from substantially smaller models, compared to the finite element method, since an approximation is induced only in the representation of the boundary conditions. Moreover, a comparison between the new technique and the conventional finite element method reveals the beneficial convergence rate of the new technique, in that it provides accurate prediction results with a substantially smaller computational effort. In this way, the new technique can be applied up to much higher frequencies than the conventional finite element method.

## 2. Basic principles

### 2.1. Problem definition

Consider the two-dimensional interior coupled vibro-acoustic problem, shown in Fig. 1. The cavity boundary surface $\Omega_a$ of an acoustic cavity with domain $V$ consists of four parts. On parts $\Omega_p$, $\Omega_v$ and $\Omega_Z$, prescribed pressure, normal velocity and normal impedance distributions are imposed, respectively, while part $\Omega_s$ consists of a flat, flexible plate with clamped boundaries ($\Omega_a = \Omega_p \cup \Omega_v \cup \Omega_Z \cup \Omega_s$). The cavity is filled with a fluid with an ambient density $\rho_0$ and speed of sound $c$. In one direction, the plate has a finite length $L$, while it is infinitely extended in the other direction.

The thickness of the plate is $t$. The plate material has the density $\rho_s$, the Poisson coefficient $\nu$, the elastic modulus $E$ and the material loss factor $\eta$. The acoustic cavity is comprised in an enclosing rectangular domain of size $L_x \times L_y$. An external normal line force $F$ is applied at position $\mathbf{r}_F(x'_F)$ on the plate. The dynamic force excitation has a harmonic time dependence with circular frequency $\omega$.

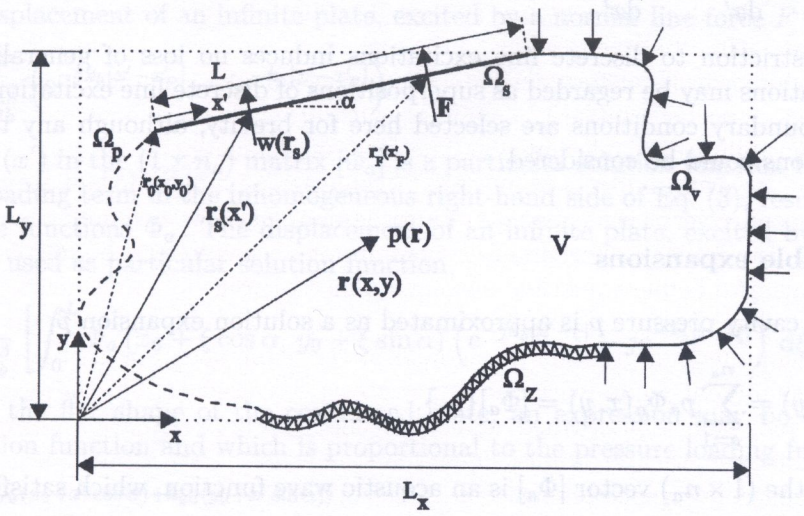


**Fig. 1.** Two-dimensional interior coupled vibro-acoustic system

The steady-state acoustic pressure $p$ at any position $\mathbf{r}(x, y)$ in the cavity domain $V$ is governed by the homogeneous Helmholtz equation,

$$\nabla^2 p(\mathbf{r}) + k^2 p(\mathbf{r}) = 0, \qquad \mathbf{r} \in V, \tag{1}$$

where $k(= \omega/c)$ is the acoustic wavenumber.

By defining a one-dimensional plate co-ordinate system $x'$ with origin at position $\mathbf{r}_0(x_0, y_0)$, as shown in Fig. 1, the geometry of the flat plate may be described by the position vector,

$$\mathbf{r}_s(x, y) = \mathbf{r}_s(x_0 + x' \cos\alpha\,,\, y_0 + x' \sin\alpha) = \mathbf{r}_s(x'). \tag{2}$$

The steady-state normal plate displacement $w$, with positive orientation away from the acoustic cavity, is governed by the inhomogeneous Kirchhoff equation for plate bending motion,

$$\frac{\mathrm{d}^4 w(x')}{\mathrm{d}x'^4} - k_b^4 w(x') = \frac{F}{D}\delta(x', x'_F) + \frac{p(x_0 + x' \cos\alpha\,,\, y_0 + x' \sin\alpha)}{D}\,, \tag{3}$$

where the structural bending wavenumber $k_b$ and the plate bending stiffness $D$ are

$$k_b = \sqrt[4]{\frac{\rho_s t \omega^2}{D}} \qquad \text{and} \qquad D = \frac{E t^3 (1 + j\eta)}{12(1 - \nu^2)}\,. \tag{4}$$

The acoustic boundary conditions for this interior coupled vibro-acoustic problem are

$$p(\mathbf{r}) = \bar{p}(\mathbf{r}), \qquad \mathbf{r} \in \Omega_p\,, \tag{5}$$

$$\frac{j}{\rho_0 \omega}\frac{\partial p(\mathbf{r})}{\partial n} = \bar{v}_n(\mathbf{r}), \qquad \mathbf{r} \in \Omega_v\,, \tag{6}$$

$$\frac{j}{\rho_0 \omega}\frac{\partial p(\mathbf{r})}{\partial n} = \frac{p(\mathbf{r})}{\bar{Z}(\mathbf{r})}, \qquad \mathbf{r} \in \Omega_Z\,, \tag{7}$$

$$\frac{j}{\rho_0 \omega}\frac{\partial p(\mathbf{r})}{\partial n} = j\omega w(\mathbf{r}), \qquad \mathbf{r} \in \Omega_s\,, \tag{8}$$

where $\bar{p}$, $\bar{v}_n$ and $\bar{Z}$ are prescribed pressure, normal velocity and normal impedance functions, respectively.

The structural clamped boundary conditions are

$$w(0) = w(L) = \frac{\mathrm{d}w(0)}{\mathrm{d}x'} = \frac{\mathrm{d}w(L)}{\mathrm{d}x'} = 0. \tag{9}$$

Note that the restriction to discrete line excitations induces no loss of generality, since general distributed excitations may be regarded as superpositions of discrete line excitations. Note also that clamped plate boundary conditions are selected here for brevity, although any type of structural boundary conditions could be considered.

### 2.2. Field variable expansions

The steady-state cavity pressure $p$ is approximated as a solution expansion $\hat{p}$,

$$p(x,y) \approx \hat{p}(x,y) = \sum_{a=1}^{n_a} p_a \Phi_a(x,y) = [\Phi_a]\{p_a\}. \tag{10}$$

Each function in the $(1 \times n_a)$ vector $[\Phi_a]$ is an acoustic wave function, which satisfies the Helmholtz equation (1),

$$\Phi_a(x,y) = \mathrm{e}^{-j(k_{xa}(x - f_{xa}.L_x) + k_{ya}(y - f_{ya}L_y))} \tag{11}$$

with

$$k_{xa}^2 + k_{ya}^2 = k^2. \tag{12}$$

In order to ensure that the amplitudes of the wave functions are not larger than 1 within the acoustic domain, which is beneficial for the numerical condition of the resulting model, the scaling factors $f_{xa}$ and $f_{ya}$ are defined as follows,

$$f_\alpha = \begin{cases} 1, & \text{if } \mathrm{Im}(k_\alpha) > 0, \\ 0, & \text{if } \mathrm{Im}(k_\alpha) \leq 0, \end{cases} \qquad (\alpha = xa, ya). \tag{13}$$

The contributions of the acoustic wave functions to the solution expansion are comprised in the $(n_a \times 1)$ vector $\{p_a\}$.

The steady-state fluid velocity vector $\vec{v}$ is approximated as

$$\vec{v} = \frac{j}{\rho_0 \omega} \vec{\nabla} p \approx \frac{j}{\rho_0 \omega} \begin{bmatrix} \dfrac{\partial \hat{p}}{\partial x} \\ \dfrac{\partial \hat{p}}{\partial y} \end{bmatrix} = \frac{j}{\rho_0 \omega} ([\partial][\Phi_a]\{p_a\}) = \frac{j}{\rho_0 \omega} ([B_a]\{p_a\}) \tag{14}$$

where $[\partial]$ is a $(2 \times 1)$ vector of gradient operators and where $[B_a]$ is a $(2 \times n_a)$ matrix of gradient components of the acoustic wave functions.

The steady-state normal plate displacement $w$ is approximated as a solution expansion $\hat{w}$,

$$w(x') \approx \hat{w}(x') = \sum_{s=1}^{4} w_s \Psi_s(x') + \sum_{a=1}^{n_a} p_a \hat{w}(x') + \hat{w}_F(x') = [\Psi_s]\{w_s\} + [\hat{w}_a]\{p_a\} + \hat{w}_F\,. \tag{15}$$

The 4 structural wave functions in the $(1 \times 4)$ vector $[\Psi_s]$ are 4 linearly independent solutions of the homogeneous part of the dynamic plate equation (3),

$$\Psi_s(x') = \mathrm{e}^{-j^s k_b (x' - f_s L)}, \qquad s = 1, \ldots, 4. \tag{16}$$

Scaling factor $f_2$ equals 1; the three others are zero. The contributions of the structural wave functions to the solution expansion are comprised in the $(4 \times 1)$ vector $\{w_s\}$.

Function $\hat{w}_F$ is a particular solution function for the mechanical force term in the right-hand side of Eq. (3). Several mathematical expressions may serve as particular solution. It is advantageous, however, to select an expression, which is already close to the physical response of the plate. Therefore, the displacement of an infinite plate, excited by a normal line force $F$ is selected [4],

$$\hat{w}_F(x') = \frac{-jF}{4Dk_b^3}\left(\mathrm{e}^{-jk_b|x'-x'_F|} - j\mathrm{e}^{-k_b|x'-x'_F|}\right). \tag{17}$$

Each function $\hat{w}_a(x')$ in the $(1 \times n_a)$ matrix $[\hat{w}_a]$ is a particular solution function for the part of the cavity pressure loading term in the inhomogeneous right-hand side of Eq. (3), resulting from one of the acoustic wave functions $\Phi_a$. The displacement of an infinite plate, excited by this distributed pressure, may be used as particular solution function,

$$\hat{w}_a(x') = \frac{-j}{4Dk_b^3}\left[\int_0^L \Phi_a\left(x_0 + \xi\cos\alpha,\, y_0 + \xi\sin\alpha\right)\left(\mathrm{e}^{-jk_b|x'-\xi|} - j\mathrm{e}^{-k_b|x'-\xi|}\right)\mathrm{d}\xi\right]. \tag{18}$$

However, due to the flat shape of the considered plate, an expression may be defined, which is a particular solution function and which is proportional to the pressure loading function,

$$\hat{w}_a(x) = \frac{\mathrm{e}^{-j(k_{xa}(x_0+x'\cos\alpha)+k_{ya}(y_0+x'\sin\alpha))}}{D\left[(k_{xa}\cos\alpha + k_{ya}\sin\alpha)^4 - k_b^4\right]}. \tag{19}$$

Although the latter expression has no direct physical meaning, it is preferred to expression (18), since it is less computationally demanding. Note that the latter expression can only be used for those acoustic wave functions, whose acoustic wavenumber components $k_{xa}$ and $k_{ya}$ are such that the denominator in Eq. (19) is non-zero.

## 2.3. Coupled vibro-acoustic wave model

Due to the particular choice of the field variable expansions (10) and (15), the governing dynamic Eqs. (1) and (3) are exactly satisfied, no matter what the values of the wave function contributions $p_a$ and $w_s$ are. These contributions are merely determined by the boundary conditions.

### *2.3.1. Structural boundary conditions*

The four structural boundary conditions (9) are defined at discrete points of the structural domain and can be used as such. Substitution of the expansions (10) and (15) yields the following matrix form of the structural boundary conditions,

$$\begin{bmatrix} C_{sa} & A_{ss} \end{bmatrix}\begin{Bmatrix} p_a \\ w_s \end{Bmatrix} = \{f_s\}. \tag{20}$$

The $(4\times4)$ matrix $[A_{ss}]$ results from the application of the differential operators, which are involved with the structural boundary conditions in Eq. (9), on the structural wave functions in the $(1 \times 4)$ vector $[\Psi_s(x')]$,

$$[A_{ss}] = \begin{bmatrix} \Psi_s(0) \\ \Psi_s(L) \\ \dfrac{\mathrm{d}\Psi_s(0)}{\mathrm{d}x'} \\ \dfrac{\mathrm{d}\Psi_s(L)}{\mathrm{d}x'} \end{bmatrix} \tag{21}$$

The $(4 \times n_a)$ coupling matrix $[C_{sa}]$ results from the application of these differential operators on the particular solution functions in the $(1 \times n_a)$ vector $[\hat{w}_a(x')]$,

$$[C_{sa}] = \begin{bmatrix} \hat{w}_a(0) \\ \hat{w}_a(L) \\ \dfrac{\mathrm{d}\hat{w}_a(0)}{\mathrm{d}x'} \\ \dfrac{\mathrm{d}\hat{w}_a(L)}{\mathrm{d}x'} \end{bmatrix} \tag{22}$$

The $(4 \times 1)$ vector $\{f_s\}$ results from the particular solution function $\hat{w}_F$,

$$\{f_s\} = \begin{Bmatrix} -\hat{w}_F(0) \\ -\hat{w}_F(L) \\ -\dfrac{\mathrm{d}\hat{w}_F(0)}{\mathrm{d}x'} \\ -\dfrac{\mathrm{d}\hat{w}_F(L)}{\mathrm{d}x'} \end{Bmatrix} \tag{23}$$

### *2.3.2. Acoustic boundary conditions*

Depending on the wave function contributions $p_a$ and $w_s$ in the field variable expansions (10) and (15), some approximation errors are induced in the representation of the acoustic boundary conditions (5)–(8). In the proposed weighted residual formulation of these boundary conditions, the involved residual error functions,

$$R_p(\mathbf{r}) = \hat{p}(\mathbf{r}) - \bar{p}(\mathbf{r}), \qquad \mathbf{r} \in \Omega_p, \tag{24}$$

$$R_v(\mathbf{r}) = \frac{j}{\rho_0 \omega} \frac{\partial \hat{p}(\mathbf{r})}{\partial n} - \bar{v}_n(\mathbf{r}), \qquad \mathbf{r} \in \Omega_v, \tag{25}$$

$$R_Z(\mathbf{r}) = \frac{j}{\rho_0 \omega} \frac{\partial \hat{p}(\mathbf{r})}{\partial n} - \frac{\hat{p}(\mathbf{r})}{\bar{Z}(\mathbf{r})}, \qquad \mathbf{r} \in \Omega_Z, \tag{26}$$

$$R_s(\mathbf{r}) = \frac{j}{\rho_0 \omega} \frac{\partial \hat{p}(\mathbf{r})}{\partial n} - j\omega \hat{w}(\mathbf{r}), \qquad \mathbf{r} \in \Omega_s, \tag{27}$$

are orthogonalized with respect to some weighting functions.

By using a weighting function $\tilde{p}$ for the residual error functions $R_v$, $R_Z$ and $R_s$ and by using a weighting function, which is proportional to the normal derivative of $\tilde{p}$, for the residual error function $R_p$, the weighted residual formulation is expressed as

$$\int_{\Omega_p} \frac{-j}{\rho_0 \omega} \frac{\partial \tilde{p}}{\partial n} R_p \, \mathrm{d}\Omega + \int_{\Omega_v} \tilde{p} R_v \, \mathrm{d}\Omega + \int_{\Omega_Z} \tilde{p} R_Z \, \mathrm{d}\Omega + \int_{\Omega_s} \tilde{p} R_s \, \mathrm{d}\Omega = 0. \tag{28}$$

In a similar way as in the Galerkin weighting procedure, used in the finite element method, the weighting function $\tilde{p}$ is expanded in terms of the same set of acoustic wave functions $\Phi_a$, used in the pressure expansion (10),

$$\tilde{p}(x, y) = \sum_{a=1}^{n_a} \tilde{p}_a \Phi_a(x, y) = [\Phi_a]\{\tilde{p}_a\}. \tag{29}$$

The substitution of the field variable expansions (10) and (15) and the weighting function expansion (29) into the weighted residual formulation (28) yields

$$\{\tilde{p}_a\}^{\mathrm{T}} \left[ ([A_{aa}] + [C_{aa}]) \{p_a\} + [C_{as}]\{w_s\} - \{f_a\} \right] = 0 \tag{30}$$

where $^{\mathrm{T}}$ denotes the transpose.

The $(n_a \times n_a)$ matrix $[A_{aa}]$ is

$$[A_{aa}] = \int_{\Omega_v+\Omega_Z+\Omega_s} \frac{j}{\rho_0\omega}[\Phi_a]^{\mathrm{T}}\{n\}^{\mathrm{T}}[B_a]\,\mathrm{d}\Omega - \int_{\Omega_p} \frac{j}{\rho_0\omega}[B_a]^{\mathrm{T}}\{n\}[\Phi_a]\,\mathrm{d}\Omega - \int_{\Omega_Z} \frac{1}{\bar{Z}}[\Phi_a]^{\mathrm{T}}[\Phi_a]\,\mathrm{d}\Omega \tag{31}$$

where the $(2 \times 1)$ vector $\{n\}$ contains the $x$- and $y$-component of the unit vector, normal to the considered boundary surface.

The $(n_a \times n_a)$ matrix $[C_{aa}]$ is

$$[C_{aa}] = -\int_{\Omega_s} j\omega[\Phi_a]^{\mathrm{T}}[\hat{w}_a]\,\mathrm{d}\Omega \tag{32}$$

and the $(n_a \times 4)$ matrix $[C_{as}]$ is

$$[C_{as}] = -\int_{\Omega_s} j\omega[\Phi_a]^{\mathrm{T}}[\Psi_s]\,\mathrm{d}\Omega. \tag{33}$$

The $(n_a \times 1)$ vector $\{f_a\}$ is

$$\{f_a\} = \{f_{ap}\} + \{f_{av}\} + \{f_{as}\} \tag{34}$$

with the $(n_a \times 1)$ vectors

$$\{f_{ap}\} = -\int_{\Omega_p} \frac{j}{\rho_0\omega}[B_a]^{\mathrm{T}}\{n\}\bar{p}\,\mathrm{d}\Omega, \tag{35}$$

$$\{f_{av}\} = \int_{\Omega v} [\Phi_a]^{\mathrm{T}}\bar{v}_n\,\mathrm{d}\Omega, \tag{36}$$

$$\{f_{as}\} = \int_{\Omega_s} j\omega[\Phi_a]^{\mathrm{T}}\hat{w}_F\,\mathrm{d}\Omega. \tag{37}$$

Since the weighted residual formulation should hold for any weighting function $\tilde{p}$, the expressions between square brackets in Eq. (30) must be zero. This yields a set of $n_a$ algebraic equations in the $(4 + n_a)$ unknown wave function contributions $w_s$ and $p_a$,

$$\left[\, C_{as} \;\; A_{aa} + C_{aa} \,\right] \left\{ \begin{matrix} w_s \\ p_a \end{matrix} \right\} = \{f_a\}. \tag{38}$$

### *2.3.3. Model properties*

The combination of the structural boundary conditions (20) and the weighted residual formulation (38) of the acoustic boundary conditions yields the coupled vibro-acoustic wave model

$$[A] \left\{ \begin{matrix} w_s \\ p_a \end{matrix} \right\} = \{b\} \tag{39}$$

with

$$[A] = \begin{bmatrix} A_{ss} & C_{sa} \\ C_{as} & A_{aa} + C_{aa} \end{bmatrix} \quad \text{and} \quad \{b\} = \left\{ \begin{matrix} f_s \\ f_a \end{matrix} \right\}. \tag{40}$$

Solving model (39) for the unknown wave function contributions $w_s$ and $p_a$ and back-substituting the results into the expansions (10) and (15) yield the prediction of the steady-state dynamic response of the coupled vibro-acoustic system.

Several model properties may be identified from the above matrix definitions.

- Since the acoustic and structural wave functions $\Phi_a$ and $\Psi_s$ are defined in, respectively, the entire acoustic domain $V$ and the entire structural domain $\Omega_s$, the model matrices are *fully populated.*
- Since the acoustic and structural wave functions $\Phi_a$ and $\Psi_s$ are complex functions and since they are implicitly dependent on frequency by virtue of the frequency dependence of their wavenumber components, the model matrices are *complex* and *frequency dependent* and cannot be partitioned into frequency independent submatrices.
- The model matrix $[A]$ is *not symmetric.* However, it is proven in [2] that the submatrix $[A_{aa}]$ is symmetric. Note that this submatrix would become the model matrix for the associated uncoupled acoustic problem, having no elastic boundary surface $\Omega_s$.

### *2.3.4. Convergence*

Since equation (12) has an infinite number of real and complex solutions, the key question is whether a set of acoustic wave functions can be selected from the infinite number of possible wave functions, such that the subsequent pressure expansion (10) converges towards the exact solution. Note that, for the considered two-dimensional case, no selection must be made regarding the structural wave functions, since the dynamic plate equation (3) has only a finite number of homogeneous, linearly independent solution functions, which are all comprised in the displacement expansion (15).

The acoustic wave functions $\Phi_a$ (see Eq. (11)) with the following wavenumber components are proposed,

$$(k_{xa}, k_{ya}) = \left(\frac{m_1\pi}{L_x}\,,\ \pm\sqrt{k^2 - k_{xa}^2}\right) \quad \text{and} \quad \left(\pm\sqrt{k^2 - k_{ya}^2}\,,\ \frac{m_2\pi}{L_y}\right), \tag{41}$$

with $m_i = 0, \pm1, \pm2, \ldots$ $(i = 1, 2)$. Recall that $L_x$ and $L_y$ are the dimensions of the (smallest) rectangular domain, enclosing the acoustic domain $V$ (see Fig. 1).

It is proven in [2] that the acoustic domain $V$ being convex is a sufficient condition for the solution expansions (10) and (15), using the proposed wave function selection (41), to converge, in the limit for $m_1, m_2 : 0 \to \infty$, towards the exact coupled vibro-acoustic response. Moreover, the contributions of each two acoustic wave functions, whose wavenumber components are based on the same $m_i$ but with opposite signs, are identical. Hence, the function set for the acoustic expansion (10) may be written as

$$\Phi_a(x, y) = \cos\left(\frac{m_1\pi}{L_x}x\right) \mathrm{e}^{-jk_{ya}(y - f_{ya}L_y)} \quad \text{and} \quad \cos\left(\frac{m_2\pi}{L_y}y\right) \mathrm{e}^{-jk_{xa}(x - f_{xa}L_x)} \tag{42}$$

with $m_i = 0, 1, 2, \ldots$ $(i = 1, 2)$.

Although a firm mathematical proof is still under construction, the authors have not yet found an example, counterproving the statement that any type of non-convex acoustic domain can be decomposed into some subdomains and that a convergent pressure expansion for each subdomain is obtained by using a wave function selection of type (41), in which $L_x$ and $L_y$ are the dimensions of a rectangular domain, enclosing the subdomain. Note that, when the acoustic domain $V$ must be decomposed for convergence reasons, some additional boundary conditions must be included to ensure the continuity of the pressure and normal fluid velocity along the common interfaces between the various subdomains.

### *2.3.5. Condition*

As it is the case for any type of Trefftz implementation [11], the coupled vibro-acoustic wave model (39) has a poor numerical condition, in that the ratio between the largest and smallest singular value of matrix $[A]$ is large. However, in contrast with the other, currently available convergent function sets [3, 7], the proposed function set (42) yields a system model, whose poor numerical

condition is not preventing the prediction results from practically converging towards the exact solutions. This may be seen, for instance, from a Picard test of the system model [9, 10]. The singular value decomposition of matrix $[A]$ takes the form

$$[A] = [U][\Sigma][V]^{\mathrm{H}} = \sum_{i=1}^{n_a+4} \{U_i\}\sigma_i\{V_i\}^{\mathrm{H}} \tag{43}$$

where $[\Sigma]$ is a diagonal matrix of singular values $\sigma_i$, where $\{U_i\}$ and $\{V_i\}$ are the $i$-th column vectors of the orthonormal matrices $[U]$ and $[V]$ and where $^{\mathrm{H}}$ denotes the complex conjugate transpose. The solution of the wave model (39) may then be written as

$$\left\{ \begin{array}{c} w_s \\ p_a \end{array} \right\} = \sum_{i=1}^{n_a+4} \frac{\{U_i\}^{\mathrm{H}}\{b\}}{\sigma_i}\{V_i\} = \sum_{i=1}^{n_a+4} \frac{\beta_i}{\sigma_i}\{V_i\}. \tag{44}$$

When a matrix has a poor numerical condition, it has several very small singular values. As may be seen from Eq. (44), the solution vector is then usually dominated by the terms, which correspond with the very small singular values and yields useless, non-converging results. However, if the coefficients $\beta_i$, associated with those very small singular values, are also very small, reliable, converging results may be obtained. In a Picard test, the singular values $\sigma_i$ are compared with their associated coefficients $\beta_i$. When the latter are smaller or at least not very much larger than their associated singular values, the problem is said to be mildly ill-conditioned, indicating that reliable results may be obtained. This is the case for the proposed wave model, as will be illustrated in the next section

## 3. Numerical validation examples

### 3.1. Validation example 1

The wave model (39) has been solved for the validation example, shown in Fig. 2. One part of the boundary surface of an air-filled ($\rho_0 = 1.225$ kg/m$^3$, $c = 340$ m/s) cavity ($L_x = 1.5$ m, $L_y = 1$ m) consists of a flexible plate ($E = 70 \times 10^9$ N/m$^2$, $\rho_s = 2790$ kg/m$^3$, $\nu = 0.3$, $t = 0.002$ m, $\eta = 0$, $L = 0.75$ m, $\alpha = 0$) with clamped boundaries, while another part of the boundary surface is treated with a layer of insulation material with normal impedance $Z = \rho_0 c(1 - 2j)$. The remaining parts of the

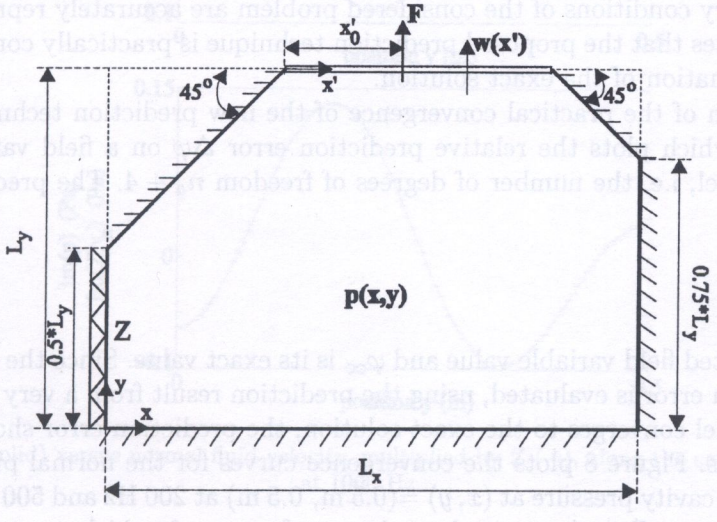


**Fig. 2.** Two-dimensional interior coupled vibro-acoustic system with a convex acoustic domain

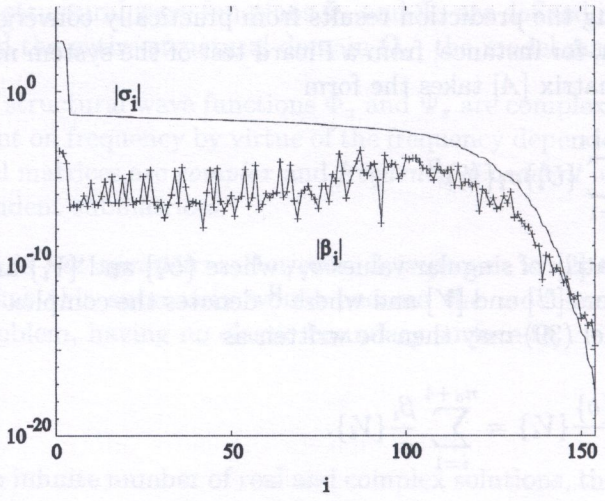


**Fig. 3.** Picard test

cavity boundary surface are perfectly rigid. The coupled vibro-acoustic system is excited by a unit normal line force $F$ at $x'_F$=0.5 m with a harmonic time dependence at frequency $\omega = 2\pi\,1000$ Hz.

As already discussed in Section 2.3.5., a necessary condition for the ill-conditioned wave model to practically converge is that it passes the Picard test. Figure 3 plots the amplitudes of the singular values $\sigma_i$ against the amplitudes of the coefficients $\beta_i$ for a wave model of the considered validation example with $n_a = 150$ acoustic wave functions. Since the coefficients $\beta_i$ gradually decrease with their associated singular values $\sigma_i$, convergence of the proposed prediction technique may be expected.

Figure 4 plots the instantaneous normal structural displacement w against the fluid displacement $w_a$, normal to the fluid–structure coupling interface, obtained from a wave model with $n_a$=660. Figure 5 compares the cavity pressure with the normal velocity, multiplied by $Z$, along the boundary surface with insulation treatment. These figures clearly indicate the accurate representation of the displacement continuity condition (8), the clamped boundary conditions (9), and the normal impedance boundary condition (7). Figures 6 and 7 show the real and imaginary parts of the cavity pressure. The fact that the pressure contour lines on these figures are perpendicular to all rigid parts of the cavity boundary surface, indicates that the rigid walled boundary condition of type (6) is accurately represented.

Since the solutions expansions (10) and (15) inherently satisfy the governing dynamic equations, and since all boundary conditions of the considered problem are accurately represented, this validation example illustrates that the proposed prediction technique is practically converging and enables an accurate approximation of the exact solution.

Another indication of the practical convergence of the new prediction technique is given by the convergence curve, which plots the relative prediction error $\Delta\varphi$ on a field variable $\varphi$ against the size of the wave model, i.e. the number of degrees of freedom $n_a + 4$. The prediction error may be defined as

$$\Delta\varphi = \frac{\|\varphi - \varphi_\infty\|}{\|\varphi_\infty\|} \tag{45}$$

where $\varphi$ is the predicted field variable value and $\varphi_\infty$ is its exact value. Since the exact solution is not known, the prediction error is evaluated, using the prediction result from a very large wave model as $\varphi_\infty$. If the wave model converges to the exact solution, the prediction error should tend to zero for increasing model sizes. Figure 8 plots the convergence curves for the normal plate displacement at $x'$=0.25m and for the cavity pressure at $(x, y)$ =(0.5 m, 0.5 m) at 200 Hz and 500 Hz for the case of an infinitely large impedance $Z$ at the cavity boundary surface $x = 0$, which means that this boundary surface is perfectly rigid. These curves confirm the convergence of the proposed wave model.

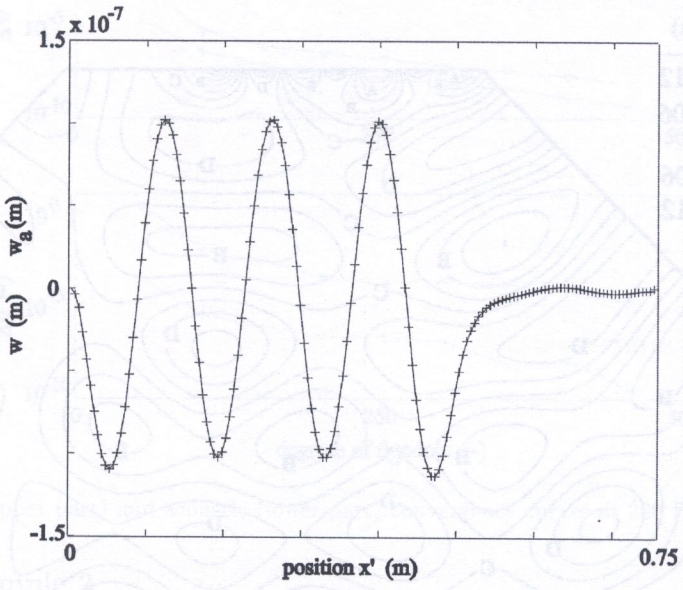


**Fig. 4.** Real part of the normal plate displacement $w$ (solid) and the normal fluid displacement $w_a$ (+)

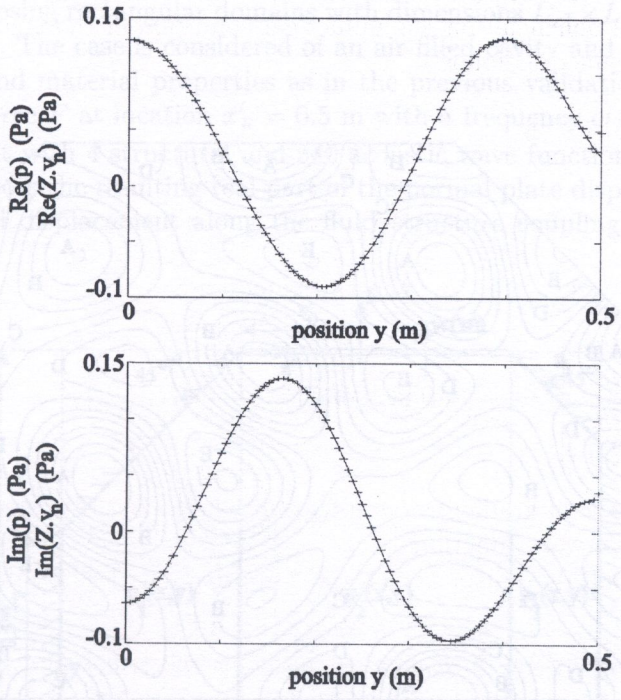


**Fig. 5.** Pressure (solid) versus normal fluid velocity, multiplied by $Z$ (+), along the cavity insulation layer at 1000 Hz

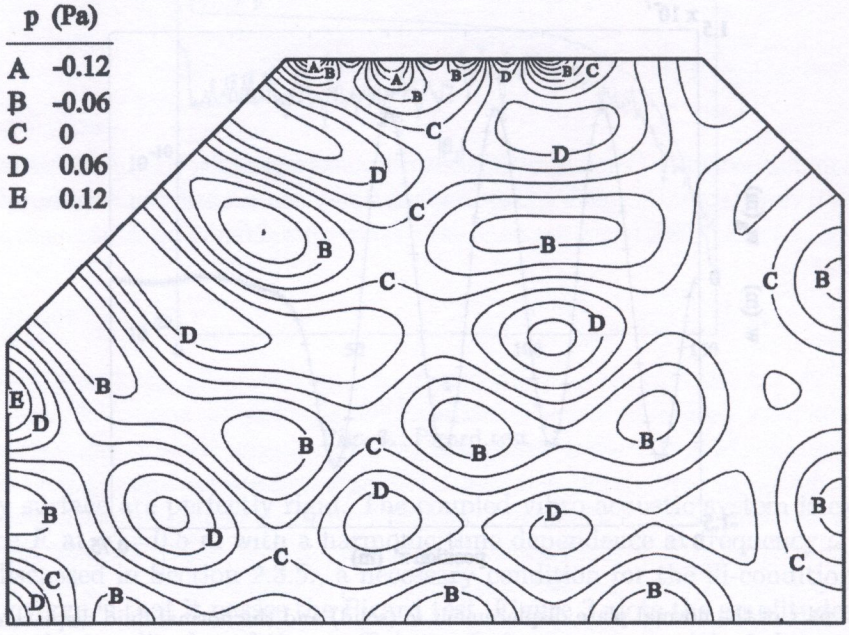


Fig. 6. Contour plot of the real part of the cavity pressure at 1000 Hz

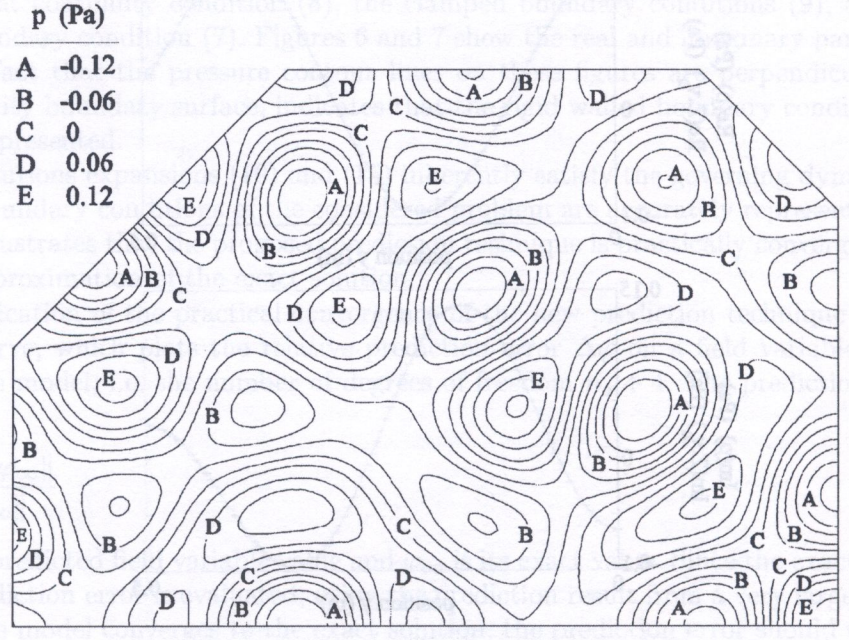


Fig. 7. Contour plot of the imaginary part of the cavity pressure at 1000 Hz

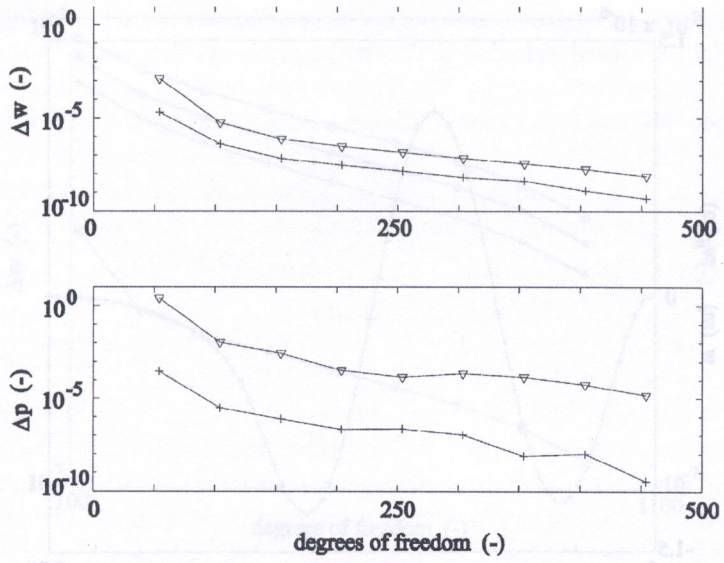


**Fig. 8.** Structural (upper part) and acoustic (lower part) convergence curves at 200 Hz (+) and 500 Hz ($\bigtriangledown$)

### 3.2. Validation example 2

Figure 9 shows an interior coupled vibro-acoustic problem, which is identical to the previous example, except that the cavity boundary surface is nowhere treated with an insulation layer and that two rigid bulkheads are positioned in the cavity domain. The bulkheads are assumed to be infinitesimally thin and their heights are $0.5 * L_y$ .

The non-convex acoustic domain is decomposed into 3 convex subdomains and the pressure fields $p_1$, $p_2$ and $p_3$ in these subdomains are expanded in terms of acoustic wave function sets (42), associated with the enclosing rectangular domains with dimensions $L_{x1} \times L_y$ , $L_{x2} \times L_y$ and $L_{x3} \times L_y$ , respectively (see Fig. 9). The case is considered of an air-filled cavity and an aluminium plate with the same geometrical and material properties as in the previous validation example. The plate is excited by a unit line force $F$ at location $x'_F = 0.5$ m with a frequency $\omega = 2\pi\, 200$ Hz.

A wave model is built with 4 structural and 540 acoustic wave functions ($n_{a1} = 180$, $n_{a2} = 210$, $n_{a3} = 150$). Figure 10 plots the resulting real part of the normal plate displacement against the real part of the normal fluid displacement along the fluid–structure coupling interface and illustrates

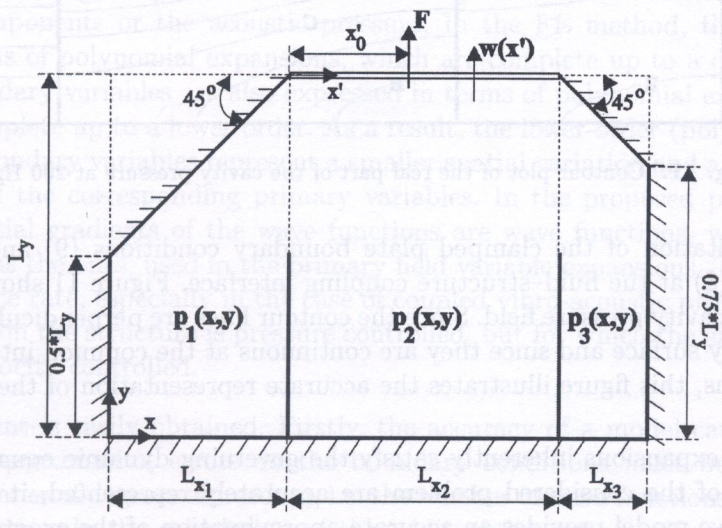


**Fig. 9.** two-dimensional interior coupled vibro-acoustic system with a non-convex acoustic domain

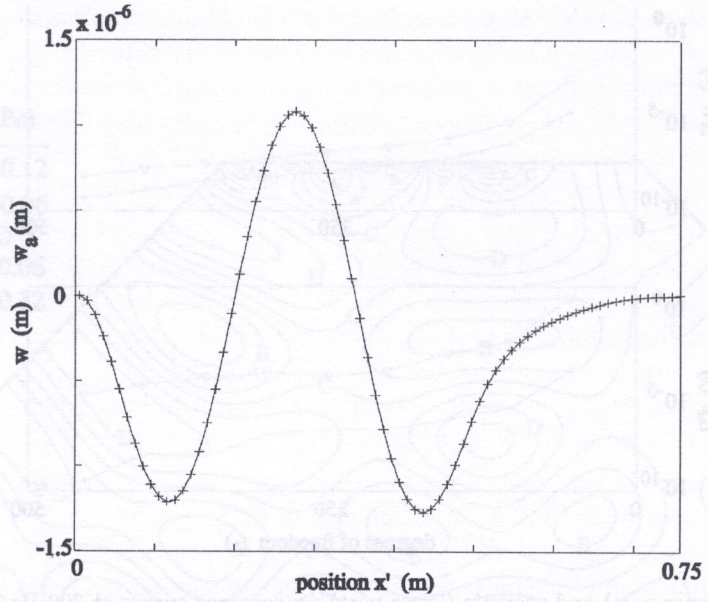


**Fig. 10.** real part of the normal plate displacement $w$ (solid) and the normal fluid displacement $w_a$ (+) along the fluid–structure coupling interface at 200 Hz

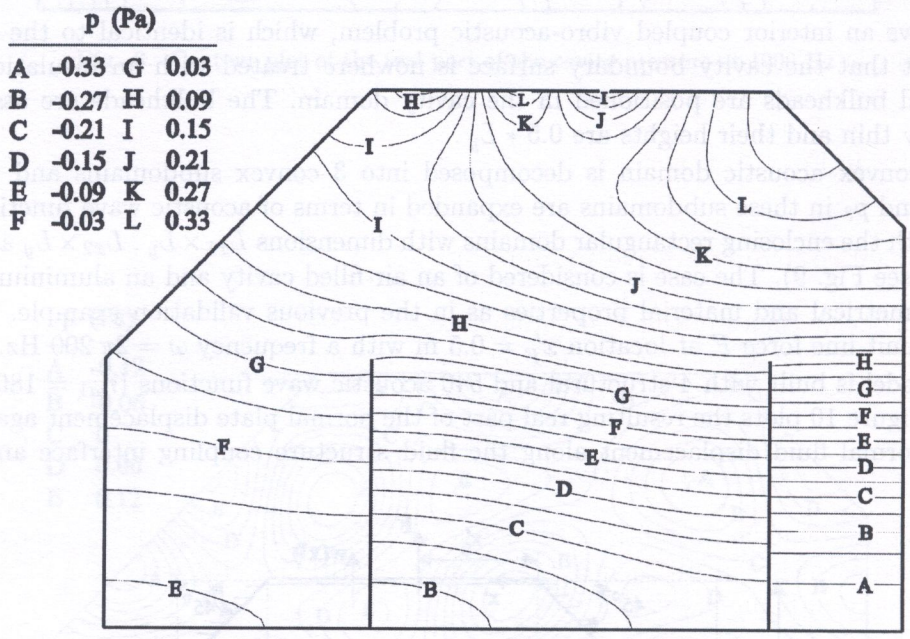


**Fig. 11.** Contour plot of the real part of the cavity pressure at 200 Hz

the accurate representation of the clamped plate boundary conditions (9) and the displacement continuity condition (8) at the fluid–structure coupling interface. Figure 11 shows the contour plot of the real part of the cavity pressure field. Since the contour lines are perpendicular to the rigid parts of the cavity boundary surface and since they are continuous at the common interfaces between the considered subdomains, this figure illustrates the accurate representation of the acoustic boundary conditions.

Since the solution expansions inherently satisfy the governing dynamic equations, and since all boundary conditions of the considered problem are accurately represented, it is illustrated again that the proposed wave model provides an accurate approximation of the exact solution. Figure 12 provides another way for indicating the practical convergence by plotting the wave model size

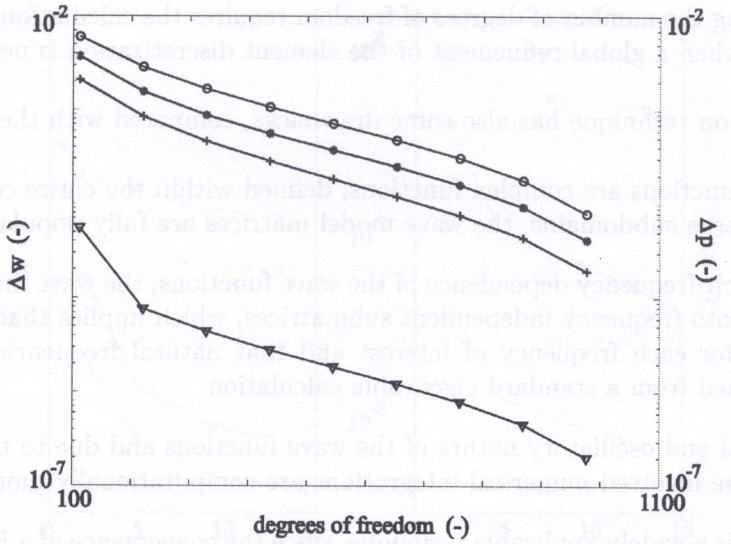


**Fig. 12.** Structural and acoustic convergence curves at 200 Hz

against the resulting relative prediction errors for the normal plate displacement predictions ($\bigtriangledown$) at $x' = 0.25$ m and for the pressure predictions at locations in the three cavity subdomains, i.e. $(x, y) = (0.2\text{m}, 0.2\text{m})$ $(+)$, $(x, y) = (1\text{m}, 0.5\text{m})$ $(\circ)$ and $(x, y) = (1.3\text{m}, 0.8\text{m})$ $(\star)$.

## 4. Comparison with FEM

### 4.1. Properties

In comparison with the finite element method, the new prediction technique has several advantageous properties.

- Since the field variable expansions satisfy a priori the governing dynamic equations, approximation errors are only involved with the representation of the boundary conditions. This yields substantially smaller models than corresponding FE models.

- Predictions of dynamic quantities such as structural stresses and strains or fluid velocities are obtained from derivating the prediction results of the primary field variables, i.e. the structural displacement components or the acoustic pressure. In the FE method, the latter are usually expressed in terms of polynomial expansions, which are complete up to a certain order. Hence, the derived secondary variables are also expressed in terms of polynomial expansions, which are however only complete up to a lower order. As a result, the lower-order (polynomial) expansions of the derived secondary variables represent a smaller spatial variation and are less accurate than the expansions of the corresponding primary variables. In the proposed prediction technique, however, the spatial gradients of the wave functions are wave functions, which have the same spatial variation as the ones, used in the primary field variable expansions. This is advantageous for the convergence rate, especially in the case of coupled vibro-acoustic problems, for which the effect of the fluid on the structure is pressure controlled, but for which the effect of the structure on the fluid is velocity controlled.

- A model refinement is easily obtained. Firstly, the accuracy of a model can be easily checked, since only the approximation errors on the boundary conditions must be verified. Secondly, increasing the number of degrees of freedom, i.e. the number of wave functions in the field variable expansions, requires only the calculation of the additional matrix coefficients, associated with the additional wave functions, while the original model coefficients remain unchanged. For FE

models, increasing the number of degrees of freedom requires the calculation of a completely new model, at least when a global refinement of the element discretization is needed.

The new prediction technique has also some drawbacks, compared with the FE method.

- Since the wave functions are complex functions, defined within the entire continuum domain or at least within large subdomains, the wave model matrices are fully populated and complex.
- Due to the implicit frequency dependence of the wave functions, the wave model matrices cannot be decomposed into frequency independent submatrices, which implies that a wave model must be recalculated for each frequency of interest and that natural frequencies and mode shapes cannot be obtained from a standard eigenvalue calculation.
- Due to the global and oscillatory nature of the wave functions and due to the poor condition of a wave model, the involved numerical integrations are computationally more demanding.
- The FE method is a widely applicable technique, since the convergence of a FE model is obtained with simple element shape functions, whereas the convergence of a wave model requires the definition of a complete wave function set and appropriate particular solution functions.

### 4.2. Computational efficiency

The new prediction technique yields accurate prediction results with substantially smaller models than the finite element method, since an approximation error is induced only on the representation of the boundary conditions. However, as indicated in the above property comparison, the beneficial effect of a smaller model size on the computational effort is partly annihilated by the fact that wave models are fully populated and cannot be decomposed into frequency-independent submatrices. Therefore, it is more appropriate for convergence comparisons to plot the relative prediction errors, as defined in (45), against the corresponding CPU times, instead of the number of unconstrained degrees of freedom.

For the validation example in Section 3.1, the results from the proposed prediction technique are compared with the results from corresponding FE models. The latter results are obtained from the MSC/NASTRAN software. A two-dimensional element discretization is obtained from one three-dimensional layer of 8-noded hexahedral fluid elements and 4-noded quadrilateral shell elements, in which the invariance in the third dimension is modelled with appropriate multiple point constraints. Table 1 lists the number of structural and acoustic elements of each FE model and their corresponding unconstrained degrees of freedom.

**Table 1.** Properties of the FE models

| | # str. elem. | # ac. elem. | dof |
|---|---|---|---|
| model 1 | 36 | 3456 | 3647 |
| model 2 | 54 | 7776 | 8063 |
| model 3 | 108 | 31104 | 31679 |
| model 4 | 135 | 48600 | 49319 |

Figure 13 shows these convergence curves for the normal plate displacement at $x' = L_{x'}/3$ and for the cavity pressure at $(x, y) = (L_x/3, L_y/2)$ for two excitation frequencies, i.e. 200 Hz and 500 Hz. The CPU times in this figure denote the times, needed for the direct response calculations at one frequency. The CPU times, plotted for the wave models, include both the times, needed for constructing the models as well as for solving the resulting matrix equations. Since FE models consist of frequency-independent submatrices, these submatrices must only be calculated once

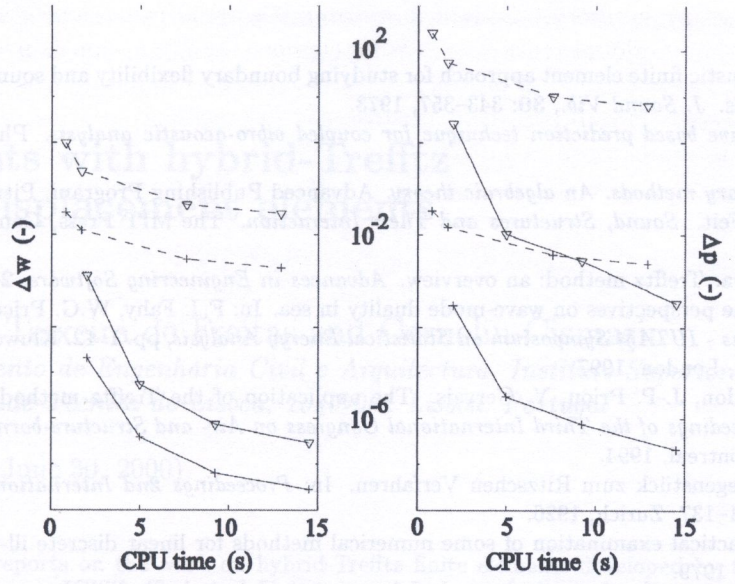


**Fig. 13.** Structural (left part) and acoustic (right part) convergence curves at 200 Hz (+) and 500 Hz (▽) (solid: wave based prediction technique, dashed: FEM)

and the construction of the models at each frequency requires only a simple submatrix assembly. As a result, the computational effort for constructing the models is negligible, compared with the efforts for solving the (large) models, at least when the dynamic response is calculated in a large frequency range. Therefore, the CPU times, plotted for the FE models, comprise only the direct solution times. All calculations are performed on a HP-C180 workstation (SPECfp95=18.7, SPECint95=11.8).

This figure illustrates the beneficial convergence rate of the new prediction technique. In comparison with the finite element method, the new prediction technique provides accurate predictions of the coupled vibro-acoustic response with a substantially smaller computational effort. Note also that the beneficial convergence rate will most likely become even more apparent, when the prediction technique is implemented in a more efficient software environment, instead of the currently used MATLAB environment.

## 5. Conclusions

A new prediction technique for coupled vibro-acoustic analysis has been developed. The technique is based on the indirect Trefftz method and approximates the structural and acoustic field variables of a coupled vibro-acoustic system in terms of solution expansions, which exactly satisfy the governing dynamic equations. The contribution factors in these expansions are obtained from a weighted residual formulation of the boundary conditions.

As it is the case for any type of Trefftz implementation, the system models of the wave based prediction technique have a poor numerical condition. However, a particular type of solution expansion has been found, which yields a system model, whose poor numerical condition is not preventing the prediction results from converging towards the exact solutions.

A comparison with the finite element method indicates that accurate prediction results may be obtained with a substantially smaller computational effort. Due to this beneficial convergence rate, the proposed prediction technique may be a suitable method for obtaining accurate coupled vibro-acoustic predictions up to much higher frequencies than the conventional finite element method.

## REFERENCES

[1] A. Craggs. An acoustic finite element approach for studying boundary flexibility and sound transmission between irregular enclosures. *J. Sound Vib.*, **30**: 343–357, 1973.

[2] W. Desmet. *A wave based prediction technique for coupled vibro-acoustic analysis.* PhD thesis, K.U. Leuven, 1998.

[3] I. Herrera. *Boundary methods. An algebraic theory.* Advanced Publishing Program. Pitman, Boston, 1984.

[4] M.C. Junger, D. Feit. *Sound, Structures and Their Interaction.* The MIT Press, Cambridge, Massachusetts, London, 1972.

[5] E. Kita, N. Kamiya. Trefftz method: an overview. *Advances in Engineering Software*, **24**: 3–12, 1987.

[6] R.S. Langley. Some perspectives on wave-mode duality in sea. In: F.J. Fahy, W.G. Price, eds., *Solid Mechanics and its Applications - IUTAM Symposium on Statistical Energy Analysis*, pp. 1–12. Kluwer Academic Publishers, Dordrecht, Boston, London, 1997.

[7] P. Masson, E. Redon, J.-P. Priou, Y. Gervais. The application of the Trefftz method to acoustics. In: M.J. Crocker, ed., *Proceedings of the Third International Congress on Air- and Structure-borne Sound and Vibration*, pp. 1809–1816, Montreal, 1994.

[8] E. Trefftz. Ein Gegenstück zum Ritzschen Verfahren. In: *Proceedings 2nd International Congress of Applied Mechanics*, pp. 131–137. Zurich, 1926.

[9] J.M. Varah. A practical examination of some numerical methods for linear discrete ill-posed problems. *SIAM Rev.*, **21**: 100–111, 1979.

[10] J.M. Varah. Pitfalls in the numerical solution of linear ill-posed problems. *SIAM J. Sci. Stat. Comput*, **4**: 164–176, 1983.

[11] A.P. Zieliński, I. Herrera. Trefftz method: fitting boundary conditions. *Int. J. Num. Meth. Eng.*, **24**: 871–891, 1987.